Journal of
Marine Science and Engineering

MDPI

Article

Optimal Constrained Control of Arrays of Wave Energy Converters

Habeebullah Abdulkadir * and Ossama Abdelkhalik

Department of Aerospace Engineering, Iowa State University, Ames, IA 50010, USA; ossama@iastate.edu
* Correspondence: habeeb19@iastate.edu

Abstract: Wave Energy Converters (WECs) are designed to be deployed in arrays, usually in a limited space, to minimize the cost of installation, mooring, and maintenance. Control methods that attempt to maximize the harvested power often lead to power flow from the WEC to the ocean, at times, to maximize the overall harvested power from the ocean over a longer period. The Power Take-Off (PTO) units that can provide power to the ocean (reactive power) are usually more expensive and complex. In this work, an optimal control formulation is presented using Pontryagin's minimum principle that aims to maximize the harvested energy subject to constraints on the maximum PTO force and power flow direction. An analytical formulation is presented for the optimal control of an array of WECs, assuming irregular wave input. Three variations of the developed control are tested: a formulation without power constraints, a formulation that only allows for positive power, and finally, a formulation that allows for finite reactive power. The control is compared with optimally tuned damping and bang–bang control.

Keywords: wave energy converter; optimal control; constrained control; reactive power; Pontryagin's minimum principle

check for updates

Citation: Abdulkadir, H.; Abdelkhalik, O. Optimal Constrained Control of Arrays of Wave Energy Converters. *J. Mar. Sci. Eng.* **2024**, *12*, 104. https://doi.org/10.3390/jmse12010104

Academic Editors: Almudena Filgueira-Vizoso and Laura Castro-Santos

Received: 27 October 2023
Revised: 28 December 2023
Accepted: 3 January 2024
Published: 5 January 2024

1. Introduction

The comparative expense of electricity produced through wave energy converters, in contrast to other renewable energy sources like wind and solar energy, stands out as a significant factor hindering the widespread adoption of ocean wave energy technology [1]. Deploying multiple WEC devices in a common area would increase the overall energy output while simultaneously leading to a reduction in the cost of installation, operation, and maintenance of the farm. The hydrodynamic interactions resulting from placing the devices close to one another can be leveraged to obtain greater energy output. In contrast to a wind farm, where the aerodynamic interaction between individual devices often results in destructive interactions, which effectively leads to the overall reduction in the performance of the array, Wave Energy Converter (WEC) arrays can be optimized to result in constructive hydrodynamic interactions between the devices [2–5].

One type of WEC is the point absorber [6,7]. Point absorbers are characterized by dimensions smaller than the wavelength of incoming waves; their efficiency is notably high when their natural frequency closely aligns with the frequency of the incident waves. Consequently, the maximum power will be generated by a point absorber when it synchronizes with the incoming wave. Control strategies implemented in wave energy converters aim to synchronize the floater's response with the excitation force on the device. Despite numerous proposed control methods over the years, they frequently overlook the intrinsic physical constraints inherent in both the floater and the Power Take-Off (PTO) units [8,9]. A significant challenge in formulating optimal controls for Wave Energy Converters (WECs) is the requirement for reactive power. This necessitates instances where a WEC contributes power to the ocean to enhance energy harvesting over an extended duration [10]. The design of the controller must account for the constraints imposed by the limited reactive power capacity of the Power Take-Off (PTO) and other physical system limitations. A PTO system providing reactive power translates to the generator also acting as a motor to drive the devices. Generally, such a PTO unit with bi-directional power capabilities will be complex and expensive.

A subset of control strategies known as passive controls completely eliminates the requirement for reactive power, as highlighted by [11]. While these controls have the advantage of not requiring reactive power, it is important to note that they typically result in a comparatively lower amount of absorbed power compared to alternative approaches, such as reactive control [12,13]. Latching control, which was proposed by Budal and Falnes [14,15], is one of the most popular passive control methods. It does not require a WEC device to return to the ocean at any point in the the process of making the system operate at resonance frequency. It works by locking the floater at some moments to keep its motion in phase with the incident wave [16]. Another widely recognized passive control method is referred to as passive loading or resistive loading, as discussed by [17]. This approach involves establishing a linear proportionality between the instantaneous value of the Power Take-Off (PTO) force and the velocity of the floater, as expressed by the equation:

$$u = -B_{pto} v$$

where $B_{pto} > 0$ is the PTO damping coefficient and v is the velocity of the floater. When the damping coefficient is adjusted to its optimal value, the corresponding control is termed Optimal Resistive Loading (ORL). The bang–bang controller is a controller that switches abruptly between the two control force extremes, as in [18]:

$$u = \begin{cases} \Upsilon, v > 0 \\ -\Upsilon, v < 0; \end{cases}$$

where $\Upsilon > 0$ is the maximum PTO force. Reference [19] recently presented two MPC control strategies designed to only allow unidirectional power flow by setting nonlinear constraints applied to a two-body point absorber. The results show that the two variations of the control developed have similar performances in terms of computational time compared to the regular MPC and obtain considerably more power than the linear passive control, thus proving to be a good option for unidirectional PTO systems.

Reactive controls, which allow for the flow of power from the WEC to the ocean, actively change the natural frequency of the device to make it closer to the resonance conditions. This type of reactive control needs to take into account limitations on the maximum possible displacements and maximum available reactive power. Numerous realistic controls have been proposed in recent research to achieve energy harvesting maximization; this can be achieved by formulating the problem as a constrained optimization problem [18,20–22]. Optimization-based controllers typically focus on maximizing absorbed power, which is defined as the product of force and velocity [23]. In a study by [24], they presented both constrained and unconstrained optimal control formulations for a single-degree-of-freedom Wave Energy Converter (WEC) device using Pontryagin's minimum principle. Notably, the constraint is not placed on power but rather on the maximum displacement of the buoy. The findings revealed that the optimal control operates in one of two modes: singular arc and bang–bang, termed the bang-singular-bang (BSB) control. Numerical results indicate that BSB control outperforms bang–bang (BB) control in terms of the amount of extracted energy. In [25], an MPC for the Wavestar wave energy converter that maximizes its power generation was presented. Two other controllers (Optimal controller and Optimal gain controller) were implemented on the wave energy absorber model for comparison.

While many of the existing controls have been developed for single WEC devices, extending these control methods to an array of devices is not straightforward because of the influence of the devices in the array on adjacent devices. Control of an array can be in two forms: either an independent control that assumes that each device is in isolation, or a collective control that accounts for the radiation and diffraction effects from the other devices. References [26,27] investigated and found that significant improvement can be obtained using a collective control compared with independent control. In the work by [28], a collective control strategy was devised for arrays of Wave Energy Converters (WECs). The control employed a Proportional-Derivative feedback control law for each WEC, incorporating optimized controller gains. To streamline the optimization process, a surrogate model composed solely of mechanical elements was employed to replace the hydrodynamic model. The outcomes of the study demonstrated that the controller effectively maximizes the energy conversion of the entire WEC array while adhering to specified constraints. Reference [29] investigated a decentralized model predictive control (MPC) to the elements of an array by considering each WEC as a subsystem. Both [30,31] applied an MPC to an array of point-absorber-type WECs; in both cases, the WEC spacing ensured inter-device interactions between the devices in the array. However, with an increase in the number of devices in a farm, the more complicated the modeling and control of the WEC array becomes. A centralized control formulation for all devices in the array was found to be too computationally expensive, which may eventually render this form of control inapplicable to for a large array. This limitation is tackled by distributing the devices on the array. The control is computed using weakly coupled hydrodynamics but the plant model takes account of the full hydrodynamic coupling. This resulted in an excellent computational efficiency for the controller.

Most of the controls available in the literature either assume a lack of bi-directional power capability or do not take into account the limitation on the bi-directional power capability of the PTOs. In this paper, an optimal control maximizing the harvested energy of the array while constraining the reactive power capability of the PTOs to a set threshold is developed. This approach leads to a practical control that does not make the device sink or slam in water; also, the control requirements do not exceed the limitations of the system. The control is derived rigorously using optimal control theory assuming irregular excitation.

There are two key contributions of this paper: First, an analytic formulation for energy-maximizing control of WEC arrays in irregular waves is developed. Second, the control developed accounts for both linear and nonlinear constraints, thereby ensuring that the resulting control does not require unrealistic amplitude motion or bi-directional power flow. The structure of this paper is outlined as follows. In Section 2, we establish the dynamic model of a simplified Wave Energy Converter (WEC) array. Section 3 details the derivation of the proposed power-constrained control formulation. Subsequently, Section 4 presents the simulation results. This paper concludes with the summarization of findings in Section 5.

2. WEC Array Dynamic Modeling

In this section, we introduce the mathematical model characterizing a Wave Energy Converter (WEC) array. This model is derived from a fundamental representation of a WEC, which is typically depicted as a second-order mass-spring-damper system. The linearized equation of motion governing an array of N devices, considering one-dimensional heave, can be expressed in time domain as [32]:

$$\boldsymbol{M}\ddot{\vec{x}}(t) = \overbrace{\int_{-\infty}^{\infty} \boldsymbol{H}_f(\tau)\vec{\eta}(t-\tau,x)d\tau}^{\text{excitation force } \vec{f}_e} + \boldsymbol{F}_s \overbrace{-\mu\ddot{x}(t) - \int_{-\infty}^{t} \boldsymbol{H}_r(\tau)\dot{\vec{x}}(t-\tau)d\tau}^{\text{radiation force } \boldsymbol{f_r}} - \vec{u}$$

where $\vec{x}$, $\dot{\vec{x}}$, $\ddot{\vec{x}}$ are the heave displacement, velocity, and acceleration vector of the buoys, respectively, and t is the time. $\boldsymbol{M}$ is the mass matrix, which contains the masses of all buoys in the array on its diagonal; $\vec{u}$ is the control force vector. $\boldsymbol{F}_s$ is the hydrostatic restoring force. The wave-exciting force on the devices is $\vec{f}_e$, where $\vec{\eta}$ is the wave surface elevation vectors at buoy's centroid. $\boldsymbol{H}_f$ is the impulse response function matrix defining the excitation force in heave. $\boldsymbol{M}_\infty$ is the added mass matrix at infinite frequency. If a body in calm water is displaced to move up and down it will generate waves. The force generated due to the radiated wave from the moving float is called the radiation force; $\boldsymbol{H}_r$ is the impulse response function matrix defining the radiation force in heave. The convolution integral is represented by a vector; a detailed formulation on the state-space approximation for the radiation terms in Equation (1) can be found in [33]:

$$\dot{x}_r = \boldsymbol{A}_r \vec{x}_r + \boldsymbol{B}_r \dot{\vec{x}} \tag{1}$$

$$\boldsymbol{F}_r = \boldsymbol{C}_r \vec{x}_r \tag{2}$$

where $\vec{x}_r \in R^{4n\times 1}$ are the radiation state vectors. $A_r \in R^{4n\times 4n}$, $B_r \in R^{4n\times 1}$, and $C_r \in R^{1\times 4n}$ are the system matrix, and input and output matrices, respectively. n represents the number of devices in the array. The dynamics of the motion of the floater can be written using Newton's law, as [8]:

$$\boldsymbol{M_t}\ddot{\vec{\boldsymbol{x}}} = \vec{f}_e(t) + \boldsymbol{C}_r \vec{x}_r + \boldsymbol{K}_h \vec{x} - \vec{u} \tag{3}$$

$\boldsymbol{M_t}$ represents the summation of the rigid body mass matrix and the added mass matrix. $\boldsymbol{C_r}$ is a matrix that contains the radiation damping coefficients, and $\boldsymbol{K}_h$ is a diagonal matrix that contains the hydrostatic forces coefficients. The hydrodynamic interaction between the WECs in the array is realized via the elements of the radiation matrices $\boldsymbol{A_r}$, $\boldsymbol{B_r}$, and $\boldsymbol{C_r}$ presented in [34,35]. The details of the formulation of these matrices are described in Section 4. The hydrodynamic matrices can be calculated for a range of finite frequencies and the infinite frequency using boundary element softwares/routines such as NEMOH [36], ANSYS Aqwa [37], and WAMIT [38].

In order to write the equation of motion in a compact state space form, we define the state vectors as follows:

$$\vec{\boldsymbol{x}} = [\vec{x}_1, \vec{x}_2, \vec{\boldsymbol{x}}_r, x_3]^T$$

where the vector $\vec{x}_1 = [x_{11}, x_{12}, x_{13}, ..., x_{1n}]^T$ is the displacement vector of the array, $\vec{x}_2 = [\dot{x}_{21}, \dot{x}_{22}, \dot{x}_{23}, ..., \dot{x}_{2n}]^T$ is the vector of velocities of all devices, and $\vec{\boldsymbol{x}}_r = [\vec{x}_{r1}, \vec{x}_{r2}, \vec{x}_{r3}, ..., \vec{x}_{rn}]^T$ is a vector containing vectors of radiation states associated with each device in the array, and because the system is a non-autonomous system, the time variable is considered as state x_3 [24]. The state-space form of the equations of motion can now be written as:

$$\begin{Bmatrix} \dot{\vec{x}}_1 \\ \dot{\vec{x}}_2 \\ \dot{\vec{x}}_r \\ \dot{x}_3 \end{Bmatrix} = \boldsymbol{A} \begin{Bmatrix} \vec{x}_1 \\ \vec{x}_2 \\ \vec{x}_r \\ x_3 \end{Bmatrix} - \boldsymbol{B}\vec{u} + \boldsymbol{B}\vec{f}_e(x_3) + \begin{bmatrix} \mathbf{0}_{(2n+4n^2)\times 1} \\ 1 \end{bmatrix} \tag{4}$$

where,

$$\boldsymbol{B} = \begin{bmatrix} \mathbf{0}_{n\times n} \\ -[\boldsymbol{M} + \boldsymbol{M}_\infty]^{-1}_{n\times n} \\ \vec{0}_{4n^2\times 1} \\ \vec{0}_{1\times n} \end{bmatrix} \tag{5}$$

$$\boldsymbol{A} = \begin{bmatrix} \mathbf{0}_{n\times n} & \boldsymbol{I}_{n\times n} & \mathbf{0}_{n\times 4n^2} & \vec{0}_{n\times 1} \\ [-[\boldsymbol{M} + \boldsymbol{M}_\infty]^{-1}\boldsymbol{K}_h]_{n\times n} & \mathbf{0}_{n\times n} & [-[\boldsymbol{M} + \boldsymbol{M}_\infty]^{-1}[\boldsymbol{C_r}_{n\times 4n^2}] & \vec{0}_{n\times 1} \\ \mathbf{0}_{4n^2\times n} & \boldsymbol{B_r}_{4n^2\times n} & \boldsymbol{A_r}_{4n^2\times 4n^2} & \mathbf{0}_{4n^2\times 1} \\ \vec{0}_{1\times n} & \vec{0}_{1\times n} & \vec{0}_{1\times 4n^2} & 0_{1\times 1} \end{bmatrix} \tag{6}$$

3. Optimal Control Formulation

The optimal control problem formulated in this section can be posed as finding the optimal control force for each device in the array such that the power from the overall array is maximized. The power from an individual device is computed as the product of the corresponding PTO control force u and the velocity of the associated floater x_2. To compute the total power in an array of WECs, power extracted by all devices is summed up to compute the cumulative power from the array. In the current formulation, the optimal control is such that the linear and nonlinear constraints are not violated. The power maximizing objective function for an array containing N number of devices can be written as [29,30]:

$$Min : J = \int_0^{t_f} \sum_{n=1}^{N} -u^n(t)x_2^n(t)dt \tag{7}$$

Subject to Equation (4),
and the constraints,

$$-\vec{\Upsilon} \leq \vec{u} \leq \vec{\Upsilon} \tag{8}$$

$$\vec{u} \circ \vec{x}_2 \geq -\vec{\epsilon} \tag{9}$$

where $\vec{u} \in \mathbb{R}_+^{N\times 1}$ is the vector of PTO control force for the N-devices in the array, $\vec{\Upsilon} \in \mathbb{R}_+^{N\times 1}$ is the control force limit. $\circ$ is the Hadamard vector product (an element-wise vector multiplication function) and $\vec{\epsilon} \in \mathbb{R}_+^{N\times 1}$ is a column vector of maximum reactive power availed by the PTO values. Following [39], we introduce a slack variable that allows for the transformation of an optimal control problem featuring a scalar control and a scalar inequality constraint into an unconstrained problem. Consequently, the inequality constraint on the control force in Equation (8) can be reformulated as an equality constraint:

$$|\vec{u}| + \vec{\beta} = \vec{\Upsilon} \tag{10}$$

where $\vec{\beta}$ is a positive slack variable. Likewise, the power constraint outlined in Equation (9) can be expressed as an equality constraint by incorporating a positive slack variable $\vec{\alpha}$, resulting in:

$$\vec{u} \circ \vec{x}_2 + \vec{\alpha} = \vec{\epsilon} \tag{11}$$

The Hamiltonian function [40] for this control problem is defined as:

$$H = -\vec{u}^T\vec{x}_2 + \vec{\lambda}_1^T\vec{x}_2 + \lambda_3 + \vec{\boldsymbol{\lambda}}_r^T(\boldsymbol{A}_r\vec{\boldsymbol{x}}_r + \boldsymbol{B}_r\vec{x}_2) + \frac{\vec{\lambda}_2^T}{[\boldsymbol{M} + \boldsymbol{M}_\infty]}\left(\vec{f}_e - \boldsymbol{C}_r\vec{\boldsymbol{x}}_r - \boldsymbol{K}_h\vec{x}_1 - \vec{u}\right) + \vec{\gamma}_1^T\left(|\vec{u}| - \vec{\Upsilon} + \vec{\beta}\right) + \vec{\gamma}_2^T(-\vec{u} \circ \vec{x}_2 - \vec{\epsilon} + \vec{\alpha}) \tag{12}$$

where the $\vec{\lambda}_1, \vec{\lambda}_2$, and $\vec{\lambda}_3$ vectors are the co-states associated with the equations of motion, and $\vec{\boldsymbol{\lambda}}_r = [\vec{\lambda}_{r1}, \vec{\lambda}_{r2}, \vec{\lambda}_{r3}, ..., \vec{\lambda}_{rn}]^T$ are the co-states of the radiation states. Finally, $\vec{\gamma}_1$ and $\vec{\gamma}_2$ are the co-state vectors associated with the PTO force constraint and the power constraint, respectively. Using the Pontryagin minimum principle, the necessary conditions for optimality can be written as:

$$\dot{\vec{\lambda}}_1^T = \vec{\lambda}_2^T[\boldsymbol{M} + \boldsymbol{M}_\infty]^{-1}\boldsymbol{K_h} \tag{13}$$

$$\dot{\vec{\lambda}}_2^T = -\vec{\lambda}_1^T - \vec{\boldsymbol{\lambda}}_r^T\boldsymbol{B}_r + \vec{u}^T + \vec{\gamma}_1{}^T \circ \vec{u}^T \tag{14}$$

$$\dot{\vec{\boldsymbol{\lambda}}}_r^T = \vec{\lambda}_2^T[\boldsymbol{M} + \boldsymbol{M}_\infty]^{-1}\boldsymbol{C}_r - \vec{\boldsymbol{\lambda}}_r{}^T\boldsymbol{A}_r \tag{15}$$

$$\dot{\lambda}_3 = -\frac{1}{[\boldsymbol{M}+\boldsymbol{M}_\infty]}\frac{\partial \vec{f}_e(x_3)}{\partial x_3}\vec{\lambda}_2^T \tag{16}$$

Differentiating H with respect to $\vec{u}$, the stationary conditions on the control force are:

$$H_u = \vec{x}_2^T + \frac{\vec{\lambda}_2^T}{[\boldsymbol{M}+\boldsymbol{M}_\infty]} + \vec{\gamma_1}^T \circ \vec{x}_2^T = 0 \tag{17}$$

As the Hamiltonian H exhibits linearity with respect to the control u, the necessary conditions of optimality fail to provide an explicit expression for the control force $\vec{u}$. This implies that the solution manifests as a singular arc control during certain time intervals. If an optimal control exists as a singular arc at some time, the input that maximizes the Hamiltonian is thus [24,41,42]:

$$u = \begin{cases} \Upsilon, H_u > 0 \\ \vec{u}_{sa}, H_u = 0 \\ -\Upsilon, H_u < 0; \end{cases}$$

These necessary equations of optimality, stationary conditions, and equations of motion are solved in the Laplace domain to obtain the singular arc control solution, $\vec{u}_{sa}$. For simplicity, if the initial condition of the states $\vec{x}_1(t_0) = 0$, $\vec{x}_2(t_0) = 0$, and $\vec{\boldsymbol{x}}_r(t_0) = 0$, then the resulting system of equations in the Laplace domain is:

$$\boldsymbol{X}_1(s) = \frac{\boldsymbol{1}}{s}\boldsymbol{X}_2 \tag{18}$$

$$s\boldsymbol{X}_1(s) = [\boldsymbol{M}+\boldsymbol{M}_\infty]^{-1}[\boldsymbol{F}_e(s) - \boldsymbol{C}_r\vec{\boldsymbol{X}}_{\boldsymbol{r}} - \boldsymbol{K}_h\boldsymbol{X}_1 - \boldsymbol{U}(s)] \tag{19}$$

$$\vec{\boldsymbol{X}}_{\boldsymbol{r}}(s) = [s\boldsymbol{I} - \boldsymbol{A}_r]^{-1}\boldsymbol{B}_r\boldsymbol{X}_2(s) \tag{20}$$

Combining Equation (18), Equation (19), and Equation (20), the state $\boldsymbol{X}_2(s)$ is solved as:

$$\boldsymbol{X}_{\boldsymbol{2}}(s) = [s^2[\boldsymbol{M}+\boldsymbol{M}_\infty] + s[\boldsymbol{C}_r[s\boldsymbol{I}-\boldsymbol{A}_r]^{-1}\boldsymbol{B}_r] + \boldsymbol{K}_h]^{-1}[s[\boldsymbol{F}_e(s) - \boldsymbol{U}(s)]] \tag{21}$$

The displacement and the radiation states can be found by substituting the solution in Equation (21) to Equations (18) and (20), respectively:

$$\boldsymbol{X}_{\boldsymbol{1}}(s) = [s^2[\boldsymbol{M}+\boldsymbol{M}_\infty] + s[\boldsymbol{C}_r[s\boldsymbol{I}-\boldsymbol{A}_r]^{-1}\boldsymbol{B}_r] + \boldsymbol{K}_h]^{-1}[\boldsymbol{F}_e(s) - \boldsymbol{U}(s)] \tag{22}$$

$$\vec{\boldsymbol{X}}_{\boldsymbol{r}}(s) = [[s\boldsymbol{I}-\boldsymbol{A}_r]^{-1}\boldsymbol{B}_r][s^2[\boldsymbol{M}+\boldsymbol{M}_\infty] + s[\boldsymbol{C}_r[s\boldsymbol{I}-\boldsymbol{A}_r]^{-1}\boldsymbol{B}_r] + \boldsymbol{K}_h]^{-1}[s[\boldsymbol{F}_e(s) - \boldsymbol{U}(s)]] \tag{23}$$

The Laplace domain transformation of the co-states equations, assuming arbitrary initial conditions are $\vec{\lambda}_1(t_0) = \vec{\lambda}_{10}$, $\vec{\lambda}_2(t_0) = \vec{\lambda}_{20}$, and $\vec{\boldsymbol{\lambda}}_r(t_0) = \vec{\boldsymbol{\lambda}}_{r0}$, is as follows:

$$\vec{\lambda}_1^T(s) = \frac{1}{s}[\vec{\lambda}_2^T[\boldsymbol{M}+\boldsymbol{M}_\infty]^{-1}\boldsymbol{K}_{\boldsymbol{h}} + \vec{\lambda}_{10}^T] \tag{24}$$

$$\vec{\lambda}_2^T(s) = \frac{1}{s}[\boldsymbol{U}^T(s) \circ (\vec{1} + \vec{\gamma_1}^T) - \vec{\lambda}_1^T(s) - \vec{\lambda}_r^T(s)\boldsymbol{B}_r + \vec{\lambda}_{20}^T(s)] \tag{25}$$

where $\vec{1}$ is used as a notation for a 1×2 row vector of ones.

$$\vec{\boldsymbol{\lambda}}_r^T(s) = \frac{1}{s}[\vec{\lambda}_2^T(s)[\boldsymbol{M}+\boldsymbol{M}_\infty]^{-1}\boldsymbol{C}_r - \vec{\lambda}_r^T(s)\boldsymbol{A}_r + \vec{\lambda}_{r0}^T(s)] \tag{26}$$

Substitute Equations (24) and (26) into Equation (25) to solve for $\vec{\lambda}_2(s)$:

$$\begin{aligned}\vec{\lambda}_2^T(s) = [s\boldsymbol{U}^T(s) \circ (\vec{1} + \vec{\gamma_1}^T) - \vec{\lambda}_{10}^T - s\vec{\lambda}_{r0}^T[s\boldsymbol{I}-\boldsymbol{A}_r]^{-1}\boldsymbol{B}_r + s\vec{\lambda}_{20}^T][s^2\boldsymbol{I} + \\ s[\boldsymbol{M}+\boldsymbol{M}_\infty]^{-1}\boldsymbol{C}_r[s\boldsymbol{I}-\boldsymbol{A}_r]^{-1}\boldsymbol{B}_r + [\boldsymbol{M}+\boldsymbol{M}_\infty]^{-1}\boldsymbol{K}_h]^{-1}\end{aligned} \tag{27}$$

Transform Equation (17) into Laplace domain, then combine with the co-state solution in Equation (27):

$$\vec{\lambda}_2^T(s) = -(\vec{1} + \vec{\gamma}_1{}^T) \circ \boldsymbol{X}_2^T(s)[\boldsymbol{M} + \boldsymbol{M}_\infty] \tag{28}$$

To simplify the presentation, let:

$$\boldsymbol{N_1} = s\vec{\lambda}_{20}^T - \vec{\lambda}_{10}^T - s\vec{\lambda}_{r0}^T[s\boldsymbol{I} + \boldsymbol{A}_r]^{-1}\boldsymbol{B}_r \tag{29}$$

$$\boldsymbol{N_2} = [s^2\boldsymbol{I} + s[\boldsymbol{M} + \boldsymbol{M}_\infty]^{-1}\boldsymbol{C}_r[s\boldsymbol{I} + \boldsymbol{A}_r]^{-1}\boldsymbol{B}_r + [\boldsymbol{M} + \boldsymbol{M}_\infty]^{-1}\boldsymbol{K}_h]^{-1} \tag{30}$$

$$\boldsymbol{N_3} = [s^2[\boldsymbol{M} + \boldsymbol{M}_\infty] + s[\boldsymbol{C}_r[s\boldsymbol{I} - \boldsymbol{A}_r]^{-1}\boldsymbol{B}_r] + \boldsymbol{K}_h]^{-1} \tag{31}$$

Substitute for $\vec{\lambda}_2^T(s)$ from Equation (28), and for $\boldsymbol{X_2}(s)$ from Equation (21) into Equation (28) to obtain:

$$[\boldsymbol{N}_3 s(\boldsymbol{F}_e(s) - \boldsymbol{U}(s))]^T = -s\boldsymbol{U}^T(s) \circ (\vec{1} + \boldsymbol{\gamma_1}^T) \times \boldsymbol{N}_2[\boldsymbol{M} + \boldsymbol{M}_\infty]^{-1} + \boldsymbol{N}_1\boldsymbol{N}_2[\boldsymbol{M} + \boldsymbol{M}_\infty]^{-1} \tag{32}$$

Rearrange Equation (32) to obtain the WEC array optimal control solution in the Laplace domain as:

$$\boldsymbol{U}(s) = \boldsymbol{U}_1(s) + \boldsymbol{U}_2(s) \tag{33}$$

$$\boldsymbol{U}_1(s) = \boldsymbol{F}_e^T(s)\boldsymbol{N}_3^T(s)\left[-\boldsymbol{N}_2[\boldsymbol{M} + \boldsymbol{M}_\infty]^{-1} + \boldsymbol{N}_3^T\right]^{-1} \tag{34}$$

$$\boldsymbol{U}_2(s) = \frac{1}{s}[(\vec{1} + \vec{\gamma}_1{}^T)\boldsymbol{N}_2[\boldsymbol{M} + \boldsymbol{M}_\infty]^{-1} + \boldsymbol{N}_3^T]^{-1} \times [\boldsymbol{N}_1\boldsymbol{N}_2[\boldsymbol{M} + \boldsymbol{M}_\infty]^{-1}]$$

$\boldsymbol{U}_2(s)$ is a function of only the initial conditions of the co-states; hence it can be dropped from the steady-state optimal control solution. The steady-state control solution is obtained as:

$$\begin{aligned} \boldsymbol{U}(s) = {} & [s[\boldsymbol{C}_r(s\boldsymbol{I} + \boldsymbol{A}_r)^{-1}\boldsymbol{B}_r - \boldsymbol{C}_r(s\boldsymbol{I} - \boldsymbol{A}_r)^{-1}\boldsymbol{B}_r]]^{-1} \\ & \times[s^2(\boldsymbol{M} + \boldsymbol{M}_\infty) + s[\boldsymbol{C}_r(s\boldsymbol{I} + \boldsymbol{A}_r)^{-1}\boldsymbol{B}_r] + \boldsymbol{K}_h]\boldsymbol{F}_e(s) \end{aligned} \tag{35}$$

The optimal control $\boldsymbol{U}(s)$ is a function of the excitation $\boldsymbol{F}_e(s)$ and the radiation state-space matrices. The inverse Laplace transform results in the time domain solution that includes unstable terms; the optimal steady-state control solution is obtained by dropping the unstable and transient terms. The time-domain singular arc solution is saturated by the maximum control force limit when the constraints are violated.

4. Numerical Simulations

To evaluate the performance of the controller developed in Section 3, an array of three identical cylindrical buoys is used, each with a radius of 2 m and draft of 3 m. The devices are laid out as in Figure 1.

The Bretschneider spectrum is considered for the generation of irregular waves with a peak period of $T_p = 4.5$ s, and significant wave height $H_s = 0.556$ m. The Bretschneider ocean wave spectrum can be computed as:

$$S(\omega) = \frac{5}{16}\frac{\omega_p^4}{\omega^5}H_s^2 e^{-5\omega_p^4/4\omega^4} \tag{36}$$

where ω is frequency in radians per second, ω_p is the significant frequency of the wave, and H_s is the significant wave height. The wave spectrum as a function of the wave frequency is plotted in Figure 2. Nemoh BEM solver is employed to compute the exact hydrodynamics for 256 equally spaced frequencies between 0.1 and 3.50 rad/s. The hydrodynamic coefficients of the array are plotted in Figures 3–5. The effect of the interactions between the devices is more noticeable in the plot of the excitation coefficients, with the forces on device one consistently larger than on the two trailing devices at all frequencies. An optimal damping control (DC) with constant PTO damping and a bang–bang control (BB) were used for comparison. The damping coefficients for the damping control were tuned for maximum performance on the same wave profile. The maximum limit of the control force provided by all PTO units is $\vec{\mathrm{Y}} = 0.1 \times Fe \approx 9 \times 10^3$ N.

We consider three possible formulations of the control:

1. An optimal control formulation with no power constraint but with a constraint on the PTO control force;
2. A passive optimal control formulation where the constraint is to allow only unidirectional power flow ($\vec{\epsilon} = 0$) and a constraint on the PTO control force;
3. A optimal control formulation where the constraint on the power flow allows for a finite negative power flow ($\vec{\epsilon} \geq 0$) and a constraint on the PTO control force.

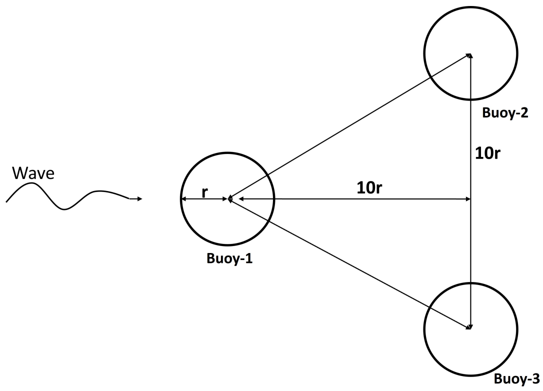

Figure 1. Layout of the devices in the array.

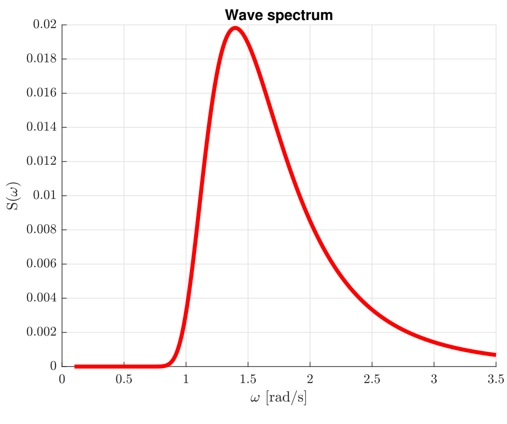

Figure 2. Wave spectrum for the considered sea state.

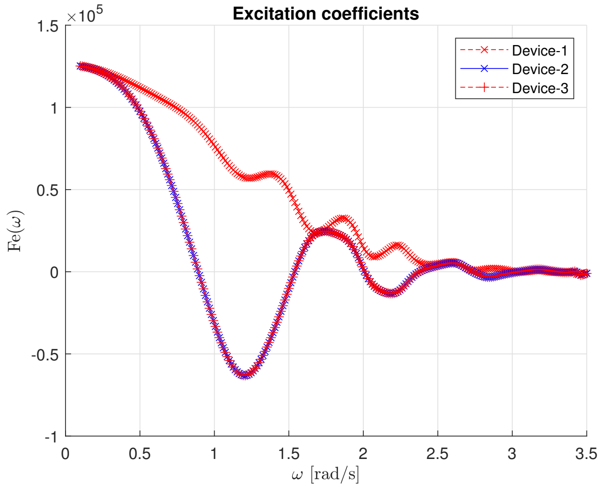

Figure 3. Excitation coefficients of the 3 devices.

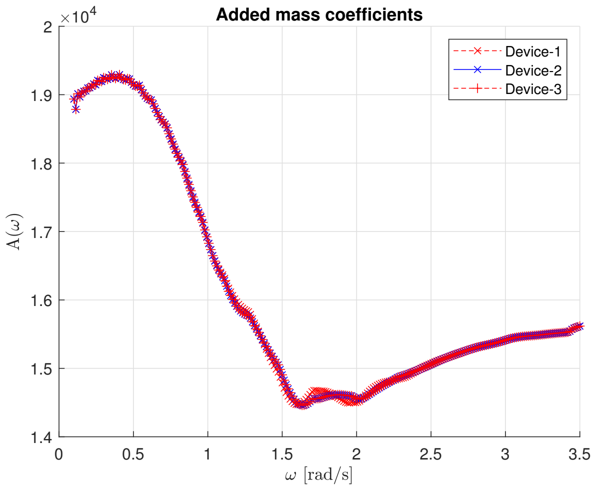

Figure 4. Added mass coefficients of the 3 devices.

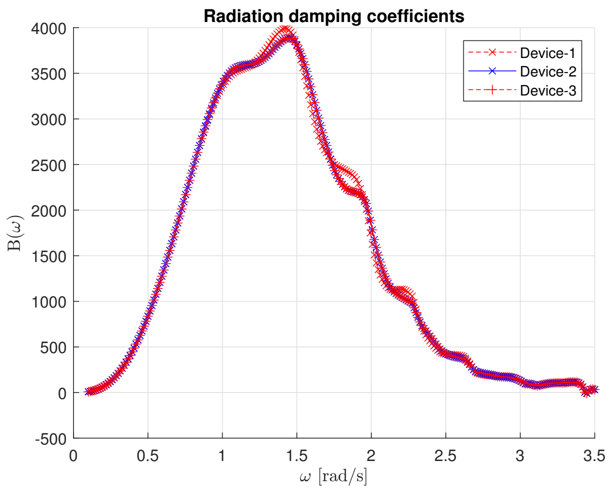

Figure 5. Radiation coefficients of the 3 devices.

4.1. No Power Constraint

It is important to highlight the need for the constraint on the power flow direction. In the current control formulation, only a linear constraint on the maximum control force is considered. The trajectory of the control force is shown in Figure 6; as can be observed, there is no violation force limit. In this figure and the following ones, it should be noted that the plot of buoys 2 and 3 are overlaid due to the symmetry of the layout along the direction of the incoming wave.

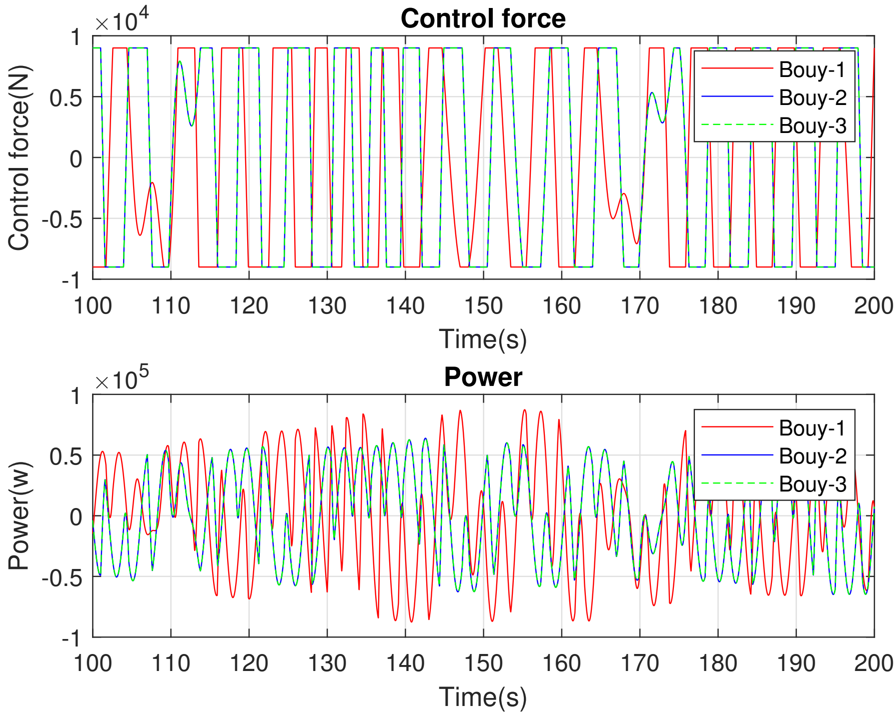

Figure 6. Control force of the power take-off units and power extracted by individual devices in the array.

The power produced by each device in the array and the total energy output of the WECs are presented in Figures 6 and 7.

The power extracted by the leading devices is relatively more significant than that extracted by the trailing devices. When above zero, the power curves represent the useful power extracted by the WEC; the negative power is the reactive component of the power. While a high magnitude of power is generated as shown in Figure 8, the overall energy harvested is not always in an upward trend due to the reactive component of the power. A PTO capable of extracting and returning the magnitude of power from/to the wave will be complex and expensive, if not impossible. For this reason and more, a constraint that accounts for the limitation on reactive power capability is needed for a practically implementable control formulation. The power flow in the array can be constrained to be unidirectional, with power flowing in the dissipative direction. However, eliminating the reactive power flow will limit the overall possible extracted power. A more optimal formulation would be to take advantage of the reactive power (if available) without exceeding the PTO system limit $\vec{\epsilon}$ as formulated in Section 3. These variations in the power constraint are investigated in the following subsections.

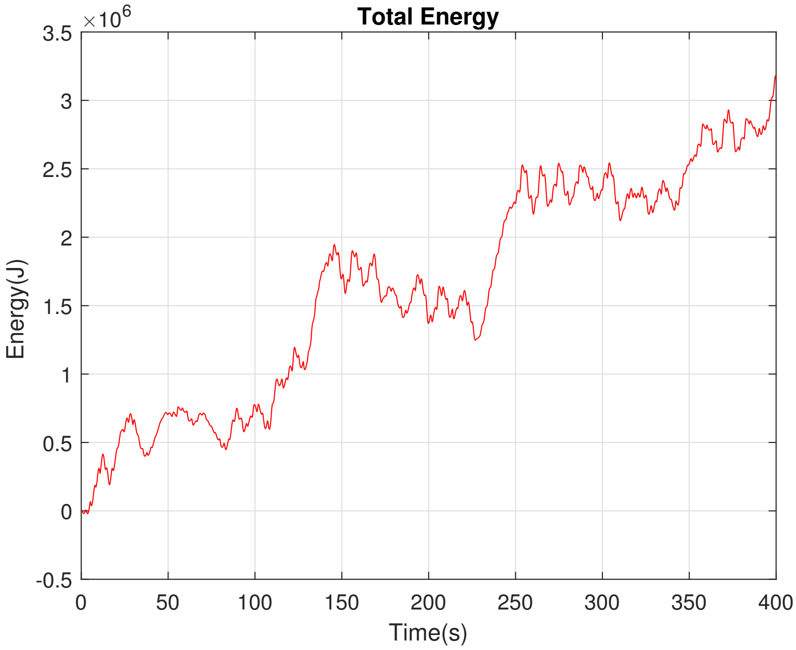

Figure 7. Total energy extracted by all the devices in the array.

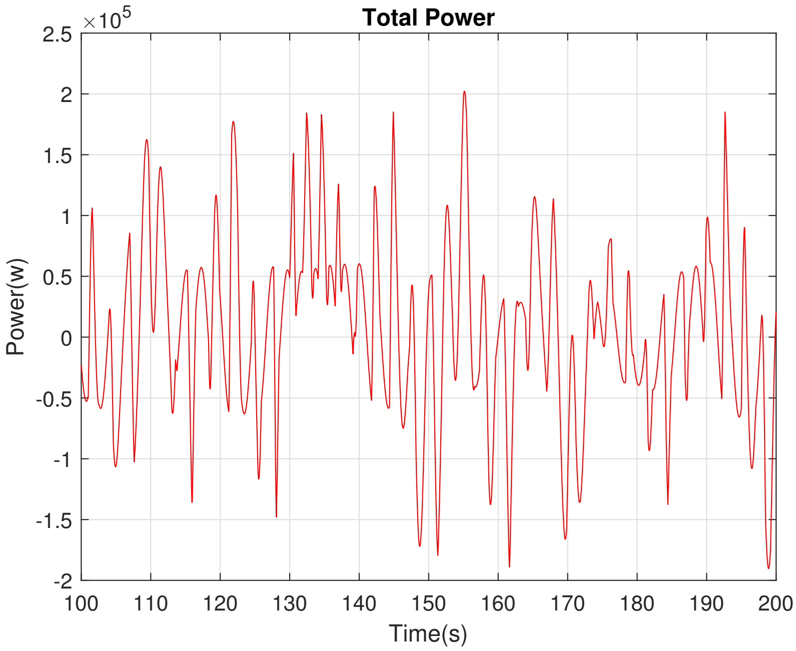

Figure 8. Cumulative power extracted by all the devices in the array.

4.2. No Reactive Power $\vec{\epsilon} = 0$

The reactive power capability of a non-ideal PTO is limited, if not non-existent. The optimal control solution of the formulation where the constraint on power is included is here referred to as the Power-Constrained Bang-Singular-Bang (PCBSB) control. This first variation is a formulation that eliminates reactive power, that is, $\vec{\epsilon} = 0$ W. This positive power formulation is compared with two other passive controls: an optimal tuned damping control (DC) and a bang–bang (BB) control, both being passive control formulations. The wave condition is the same as in the previous section. The constraint on the maximum control force provided by all PTO remains $\vec{\Upsilon} = 9 \times 10^3$ N.

The displacements and velocities experienced by the devices when controlled by the DC, BB, and the developed PCBSB control are plotted in Figures 9 and 10, respectively. Figure 11 shows the total combined power from the array. The DC, BB, and the current formulation of the PCBSB, all being passive controls, do not require reactive power. Therefore, the power curve does not go below zero. Figure 12 shows the trajectory of the DC, BB, and PCBSB controls when implemented on the array. The BB control is an on–off controller, which can only take one of two fixed-value switches between the maximum and minimum limits of the control force. The PCBSB control, on the other hand, has an SA solution when the force saturation and power constraints are not violated.

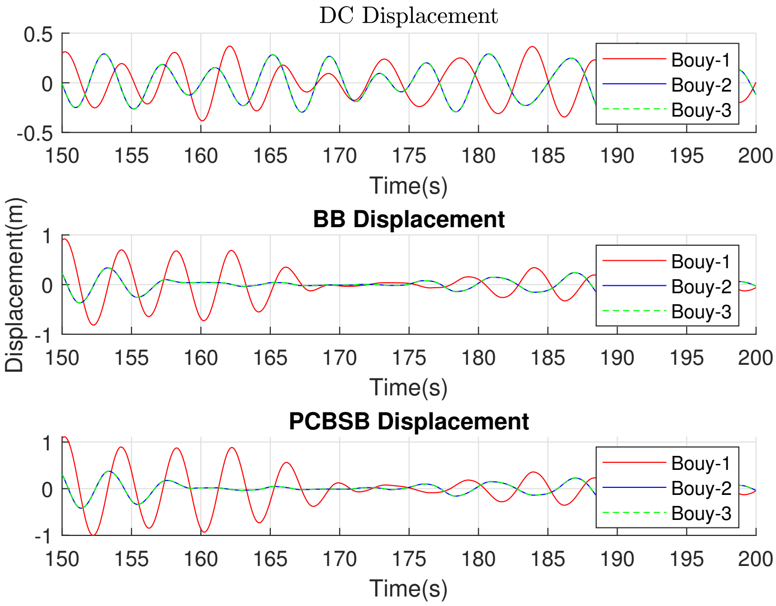

Figure 9. Displacement of all buoys when being controlled using damping control, bang–bang control, and the power-constrained bang-singular-bang control.

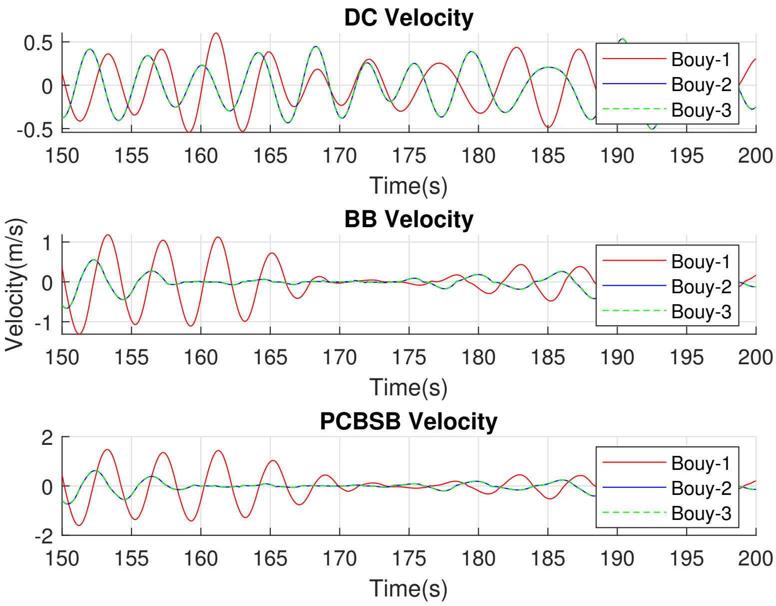

Figure 10. Velocity of all buoys when being controlled using damping control, bang–bang control, and the power-constrained bang-singular-bang control.

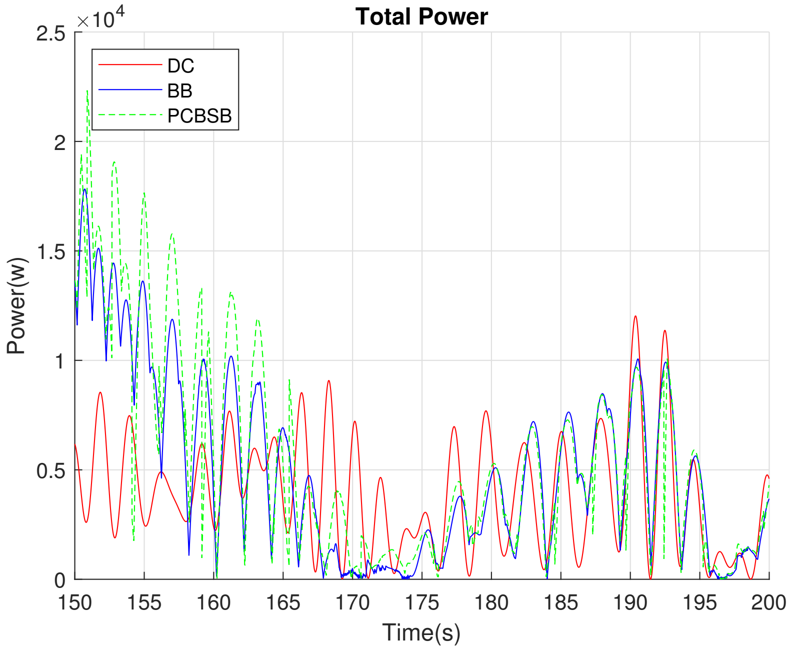

Figure 11. Power extracted by all devices when being controlled using damping control, bang–bang control, and the power-constrained bang-singular-bang control.

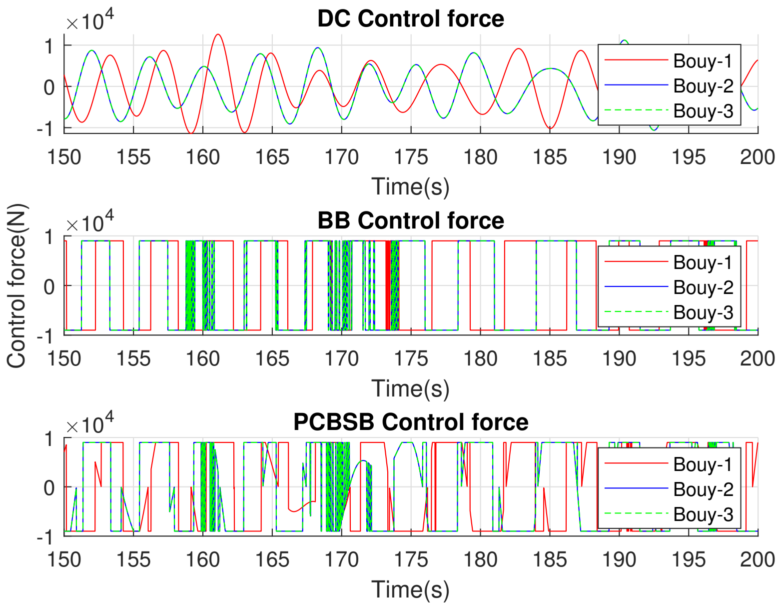

Figure 12. Control force trajectory of the PTO values when being controlled using damping control, bang–bang control, and the power-constrained bang-singular-bang control.

As observed in Figure 13, the overall energy harvested using PCBSB control is significantly higher than that of both DC and BB controls. A 5.11% and 12.36% increase in overall energy extracted from the array was achieved using the PCBSB compared with BB and DC control, respectively. The performance of the PCBSB can be further improved by assuming the PTO has the capability to provide a finite amount of reactive power capability. To further understand the performance of the controllers, the non-dimensional capture width ratio (CWR) is computed. CWR is defined as [30]:

$$CWR = \frac{P_{absorbed}}{P_{wave}} = \frac{1}{2r}\frac{P_{av}/N}{P_{wave}}$$

where $P_{wave} = \frac{1}{2}\rho g \int_{\omega_{min}}^{\omega_{max}} \frac{S(\omega)}{\omega} d\omega$ is the incident irregular wave power flux [43], P_{av} is the time-averaged total power from the array, r is the device radius, and N is the number of devices in the array. The CWRs of the devices when the array is controlled using DC, BB, and PCBSB controls are 0.2890, 0.3088, and 0.3247, respectively.

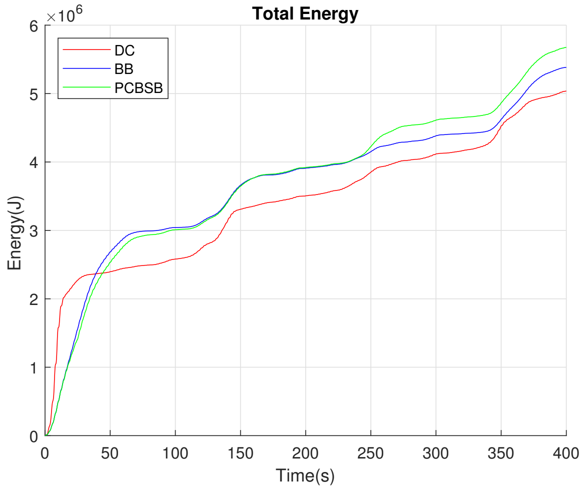

Figure 13. Total energy extracted from the waves when the devices are being controlled using damping control, bang–bang control, and the power-constrained bang-singular-bang control.

4.3. Finite Reactive Power $\vec{\epsilon} \geq 0$

In this formulation, the PCBSB solution allows for a set finite amount of reactive power, that is, $\vec{\epsilon} \geq 0$ W. We assume a reactive power limit, $\vec{\epsilon} = 0.5 \times 10^4$ W is tested with the same wave condition and maximum control constraint considered in the previous section. The improvements are measured against the passive DC and BB controls.

In Figure 14, the total power generated by the device when controlled using DC and BB is plotted in the top plot, and the power generated by the individual devices when controlled using the PCBSB is plotted in the lower plot for clarity. It can be observed that the PCBSB power plot goes below the zero line but without exceeding the set limit. Similar to the passive power constraint formulation in the preceding section, Figure 15 shows the trajectory of the PCBSB control when implemented on the array being an SA solution when the force saturation and power constraints are not violated.

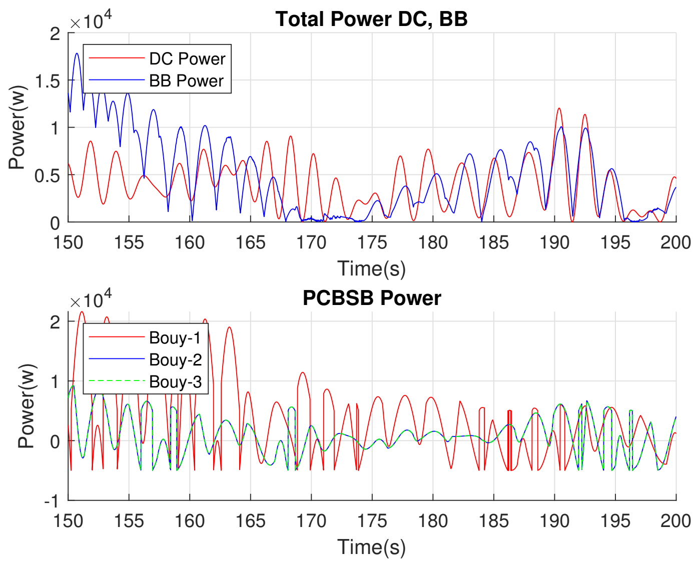

Figure 14. Power extracted using PTO units when being controlled using damping control, bang–bang control, and the power-constrained bang-singular-bang control.

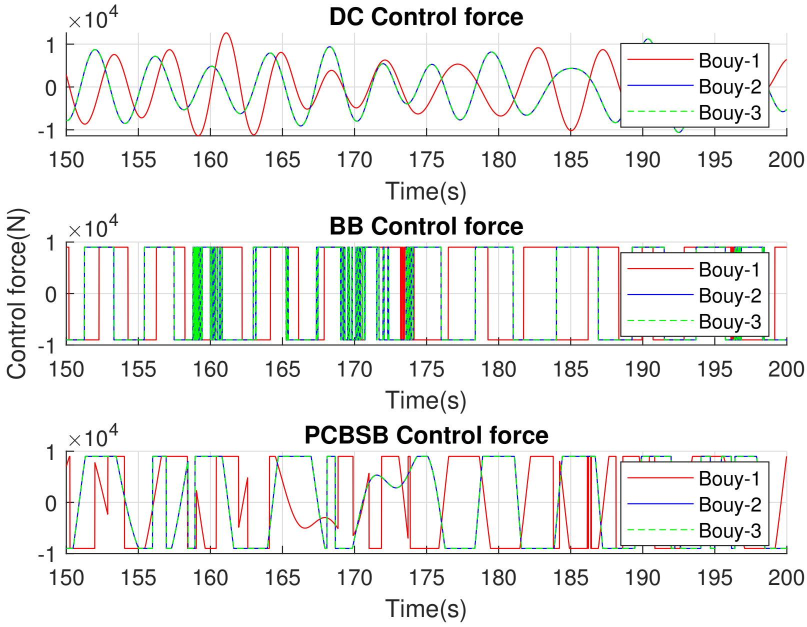

Figure 15. Control force trajectories when being controlled using damping control, bang–bang control, and the power-constrained bang-singular-bang control.

An overall increase in energy harvested of 24.14% is achieved using PCBSB control compared with BB control is presented in Figure 16. The energy extraction can be further improved by increasing the reactive power capability, although, as the reactive power threshold grows towards that required by the singular arc control, so does the complexity of the PTO system. The CWR of the array when being controlled using the PCBSB control is improved to 0.3832.

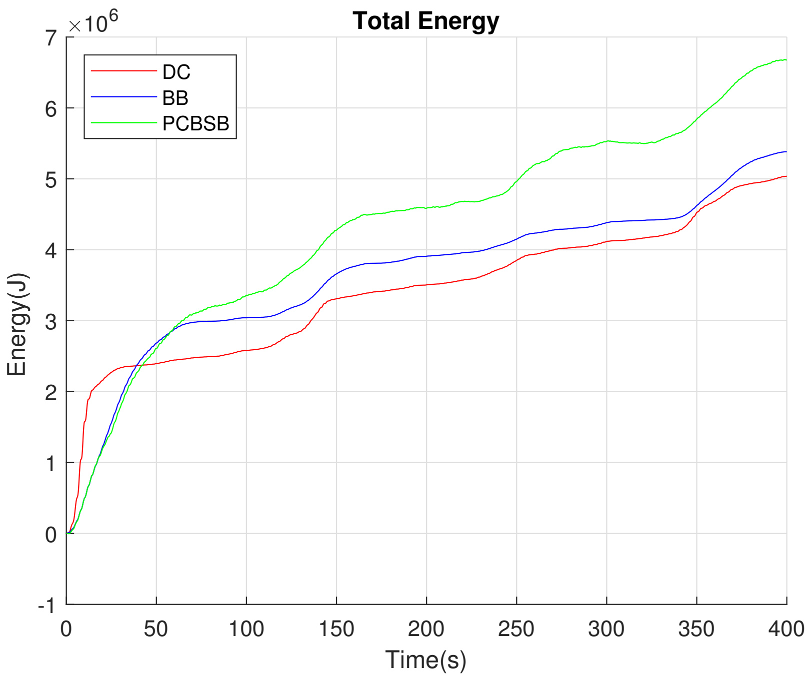

Figure 16. Total energy extracted by the devices when being controlled using damping control, bang–bang control, and the power-constrained bang-singular-bang control with $\vec{\epsilon} = 0.5 \times 10^4$ W.

5. Conclusions

In this paper, we proposed constrained optimal control formulation for an array of WECs. The control with linear and nonlinear constraints on PTO control force and power flow direction was derived analytically within the context of optimal control theory for an array of WECs with irregular excitation. To test the performance of the control, three formulations were tested: I) the performance of the control solution when the only constraint is on the PTO force (this was investigated to demonstrate the need for power constraints), II) the unidirectional power-constrained control, and III) the formulation that allows for finite reactive power. The performance of the controls was compared to optimally tuned damping control (DC) and bang–bang (BB) control.

Through simulations, we showed the reactive power requirements of the unconstrained reactive control formulation. Then, the performance of the optimal control solution when it is assumed to have no reactive power was compared with damping control and bang–bang control. Finally, we tested a formulation that allows for an arbitrary amount of limited reactive power in order to demonstrate the capabilities of the control to handle varying amounts of reactive power. Overall, the proposed power-constrained bang-singular-bang control was found to exhibit optimal energy extraction by leveraging the hydrodynamic coupling between the devices to maximize the power output. Future research will concentrate on testing the control formulation on a test array in a wave tank.

Author Contributions: Conceptualization, O.A.; methodology, H.A. and O.A.; software, H.A. and O.A.; validation, H.A. and O.A.; resources, O.A.; writing—original draft preparation, H.A.; writing—review and editing, H.A. and O.A.; supervision, O.A.; project administration, O.A.; funding acquisition, O.A. All authors have read and agreed to the published version of the manuscript.

Funding: This paper is based upon work supported by NSF, Grant Number 2048413. The research reported in this paper is partially supported by the HPC@ISU equipment at Iowa State University, some of which has been purchased through funding provided by NSF under MRI grant number 1726447.

Institutional Review Board Statement: Not applicable.

Informed Consent Statement: Not applicable.

Data Availability Statement: All data generated or analyzed during the study of this manuscript are included in the article.

Conflicts of Interest: With respect to the content of this paper, all the authors have no conflicts of interest to declare.

References

1. Foteinis, S. Wave energy converters in low energy seas: Current state and opportunities. *Renew. Sustain. Energy Rev.* **2022**, *162*, 112448. [CrossRef]
2. Engström, J.; Eriksson, M.; Göteman, M.; Isberg, J.; Leijon, M. Performance of large arrays of point absorbing direct-driven wave energy converters. *J. Appl. Phys.* **2013**, *114*, 204502. [CrossRef]
3. Howey, B.; Collins, K.M.; Hann, M.; Iglesias, G.; Gomes, R.P.; Henriques, J.C.; Gato, L.M.; Greaves, D. Compact floating wave energy converter arrays: Inter-device mooring connectivity and performance. *Appl. Ocean Res.* **2021**, *115*, 102820. [CrossRef]
4. Folley, M. *Numerical Modelling of Wave Energy Converters: State-of-the-Art Techniques for Single Devices and Arrays*; Academic Press: Cambridge, CA, USA, 2016.
5. Tian, W.; Wang, Y.; Shi, W.; Michailides, C.; Wan, L.; Chen, M. Numerical study of hydrodynamic responses for a combined concept of semisubmersible wind turbine and different layouts of a wave energy converter. *Ocean Eng.* **2023**, *272*, 113824. [CrossRef]
6. Brekken, T.K. On model predictive control for a point absorber wave energy converter. In Proceedings of the 2011 IEEE Trondheim PowerTech, Trondheim, Norway, 19–23 June 2011; pp. 1–8.
7. Pastor, J.; Liu, Y. Frequency and time domain modeling and power output for a heaving point absorber wave energy converter. *Int. J. Energy Environ. Eng.* **2014**, *5*, 1–13. [CrossRef]
8. Faedo, N.; Olaya, S.; Ringwood, J.V. Optimal control, MPC and MPC-like algorithms for wave energy systems: An overview. *IFAC J. Syst. Control* **2017**, *1*, 37–56. [CrossRef]
9. Faedo, N.; Scarciotti, G.; Astolfi, A.; Ringwood, J.V. Moment-based constrained optimal control of an array of wave energy converters. In Proceedings of the 2019 American Control Conference (ACC), Philadelphia, PA, USA, 10–12 July 2019; pp. 4797–4802.

10. Falnes, J. *Ocean Waves and Oscillating Systems—Linear Interactions Including Wave-Energy Extraction*; Cambridge University Press: Cambridge, UK, 2002; Chapter 4.
11. Shabara, M.A.; Abdelkhalik, O. Dynamic Modeling of Spherical Variable-Shape Wave Energy Converters. *arXiv* **2022**, arXiv:2201.08942.
12. Son, D.; Yeung, R.W. Real-time implementation and validation of optimal damping control for a permanent-magnet linear generator in wave energy extraction. *Appl. Energy* **2017**, *208*, 571–579. [CrossRef]
13. Garcia-Rosa, P.B.; Kulia, G.; Ringwood, J.V.; Molinas, M. Real-time passive control of wave energy converters using the Hilbert-Huang transform. *IFAC-PapersOnLine* **2017**, *50*, 14705–14710. [CrossRef]
14. Budar, K.; Falnes, J. A resonant point absorber of ocean-wave power. *Nature* **1975**, *256*, 478. [CrossRef]
15. Budal, K.; Falnes, J. Optimum operation of improved wave-power converter. *Mar. Sci. Commun.* **1977**, *3*, 2. Available online: https://www.osti.gov/biblio/7213955 (accessed on 3 September 2023) .
16. Henriques, J.; Lopes, M.; Gomes, R.; Gato, L.; Falcão, A. On the annual wave energy absorption by two-body heaving {WECs} with latching control. *Renew. Energy* **2012**, *45*, 31–40. [CrossRef]
17. Nielsen, K.M.; Pedersen, T.S.; Andersen, P.; Ambühl, S. Optimizing control of wave energy converter with losses and fatigue in power take off. *IFAC-PapersOnLine* **2017**, *50*, 14680–14685. [CrossRef]
18. Li, G.; Weiss, G.; Mueller, M.; Townley, S.; Belmont, M.R. Wave energy converter control by wave prediction and dynamic programming. *Renew. Energy* **2012**, *48*, 392–403. [CrossRef]
19. Montoya, D.; Tedeschi, E.; Castellini, L.; Martins, T. Passive Model Predictive Control on a Two-Body Self-Referenced Point Absorber Wave Energy Converter. *Energies* **2021**, *14*, 1731. [CrossRef]
20. Hals, J.; Falnes, J.; Moan, T. Constrained optimal control of a heaving buoy wave-energy converter. *J. Offshore Mech. Arct. Eng.* **2011**, *133*, 011401. [CrossRef]
21. Bacelli, G.; Ringwood, J. Constrained control of arrays of wave energy devices. *Int. J. Mar. Energy* **2013**, *3–4*, e53–e69. [CrossRef]
22. Chen, M.; Xiao, P.; Zhang, Z.; Sun, L.; Li, F. Effects of the end-stop mechanism on the nonlinear dynamics and power generation of a point absorber in regular waves. *Ocean Eng.* **2021**, *242*, 110123. [CrossRef]
23. Wilson, D.; Bacelli, G.; Coe, R.G.; Bull, D.L.; Abdelkhalik, O.; Korde, U.A.; Robinett, R.D., III. *A Comparison of WEC Control Strategies*; Sandia National Laboratories Tech. Rep. SAND2016-4293; Sandia National Laboratories (SNL-NM): Albuquerque, NM, USA, 2016; Voloume 10, p. 1431291.
24. Zou, S.; Abdelkhalik, O.; Robinett, R.; Bacelli, G.; Wilson, D. Optimal control of wave energy converters. *Renew. Energy* **2017**, *103*, 217–225. [CrossRef]
25. Soltani, M.N.; Sichani, M.T.; Mirzaei, M. Model Predictive Control of Buoy Type Wave Energy Converter. In Proceedings of the 19th International Federation of Automatic Control (IFAC) World Congress, Cape Town, South Africa, 25–29 August 2014.
26. Westphalen, J.; Bacelli, G.; Balitsky, P.; Ringwood, J. Control strategies for arrays of wave energy devices. In Proceedings of the 9th European Wave and Tidal Energy Conference (EWTEC), School of Civil Engineering and the Environment, Southampton, UK, 5–9 September 2011.
27. Bacelli, G.; Balitsky, P.; Ringwood, J.V. Coordinated control of arrays of wave energy devices—Benefits over independent control. *IEEE Trans. Sustain. Energy* **2013**, *4*, 1091–1099. [CrossRef]
28. Zou, S.; Abdelkhalik, O. Collective control in arrays of wave energy converters. *Renew. Energy* **2020**, *156*, 361–369. [CrossRef]
29. Oetinger, D.; Magaña, M.E.; Sawodny, O. Decentralized model predictive control for wave energy converter arrays. *IEEE Trans. Sustain. Energy* **2014**, *5*, 1099–1107. [CrossRef]
30. Zhong, Q.; Yeung, R.W. On optimal energy-extraction performance of arrays of wave-energy converters, with full consideration of wave and multi-body interactions. *Ocean Eng.* **2022**, *250*, 110863. [CrossRef]
31. Li, G.; Belmont, M. Model predictive control of an array of wave energy converters. In Proceedings of the 11th European Wave and Tidal Energy Conference, EWTEC, Aalborg, Denmark, 2–5 September 2013.
32. Cummins, W.; Iiuhl, W.; Uinm, A. The impulse response function and ship motions. In Proceedings of the Symposium on Ship Theory, Hamburg, Germany, 25–27 January 1962.
33. Jefferys, E. Simulation of wave power devices. *Appl. Ocean Res.* **1984**, *6*, 31–39. [CrossRef]
34. Lyu, J. Optimization and Control of Arrays of Wave Energy Converters. Ph.D. Thesis, Michigan Technological University, Houghton, MI, USA, 2019.
35. Zou, M.; Chen, M.; Zhu, L.; Li, L.; Zhao, W. A constant parameter time domain model for dynamic modelling of multi-body system with strong hydrodynamic interactions. *Ocean Eng.* **2023**, *268*, 113376. [CrossRef]
36. Babarit, A.; Delhommeau, G. Theoretical and numerical aspects of the open source BEM solver NEMOH. In Proceedings of the 11th European Wave and Tidal Energy Conference (EWTEC2015), Nantes, France, 6–11 September 2015.
37. ANSYS. *AQUA*; Version 15.0; ANSYS. Inc.: Canonsburg, PA, USA, 2013; Volume 752.
38. *WAMIT User Manual, V. 7.0*; WAMIT Inc.: Chestnut, MA, USA, 2013.
39. Jacobson, D.; Lele, M. A transformation technique for optimal control problems with a state variable inequality constraint. *IEEE Trans. Autom. Control* **1969**, *14*, 457–464. [CrossRef]
40. Bryson, A.E.; Ho, Y.C. *Applied Optimal Control: Optimization, Estimation, and Control*; Routledge: London, UK, 2018.
41. Hendrikx, R.; Leth, J.; Andersen, P.; Heemels, W. Optimal control of a wave energy converter. In Proceedings of the 2017 IEEE Conference on Control Technology and Applications (CCTA), Kohala Coast, HI, USA, 27–30 August 2017; pp. 779–786.

42. Abraham, E. Optimal Control And Robust Estimation for Ocean Wave Energy Converters. Ph.D. Thesis, Department of Aeronautics, Imperial College London, London, UK, 2013.
43. Rogne, Ø.Y. Numerical and Experimental Investigation of a Hinged 5-Body Wave Energy Converter. Ph.D. Thesis, Norwegian University of Science and Technology, Trondheim, Norway, 2014 .